Possible Self-Arresting Screening Current Stress Damage in a REBCO Test Coil at 42.6 T in 31 T Background Field

Jonathan Lee, Jeseok Bang, Garfield Murphy, Griffin Bradford, Cade Watson, Kwangmin Kim, Jan Jaroszynski, Rastislav Ries, Aixia Xu, Anatolii Polyanskii, Najib Cheggour, and David Larbalestier, *Life Fellow, IEEE*

***Abstract*—REBCO coated conductors (CCs) have now been optimized for current-carrying capacity in high magnetic fields. Production-length CCs may carry more than 1500 A at 4.2 K/30 T in the $B//ab$ configuration. Such high I_c is essential for the construction of new generations of ultra-high field ($B > 40$ T) magnets. However, high I_c also increases screening current stresses (SCS) and makes these contemporary tapes vulnerable to mechanical damage during magnet operation. To study this vulnerability, we constructed and tested Little Big Coil #6 (LBC6), one of a series of standardized ultra-high field insert coils operated in a 31 T resistive background field at the National High Magnetic Field Laboratory (NHMFL). LBC6 used contemporary conductor with triple the I_c of the earlier LBCs, so we hypothesized that the coil would be destroyed by SCS during operation. Instead, LBC6 survived multiple quenches from more than 42 T and repeated cycling from 31 T to 41 T. Postmortem analysis revealed plastic deformation throughout the winding pack, but the damage to the REBCO layer was confined to one conductor edge. We propose that this coil exhibited a self-arresting damage mechanism: during the initial energization and quench, SCS damage sufficiently narrowed the superconducting filament width (thus reducing I_c) such that no further SCS damage occurred during subsequent operation. Possible implications for ultra-high-field magnet design are discussed.**

***Index Terms*—REBCO coated conductor, screening currents, no-insulation magnet, ultra-high field.**

I. Introduction

In REBCO magnets, any radial field can induce persistent screening currents within the wide superconducting filament of the REBCO coated conductor (CC). Screening currents circulate at $\pm J_c$ and thus produce local hoop stresses on the order of $\pm J_e B r$ even at operating currents $I_{op} \ll I_c$. These local hoop stresses, usually referred to as screening current stresses (SCS), dominate the mechanical stress state in REBCO magnets during regular, non-quench operations.

Several approaches exist for SCS management, including mechanical reinforcement techniques [1], [2] or controlled cooling schemes to enforce $J_{e,op} \sim J_e(B,T,\theta)$ during charging [3]. However, SCS mitigation is complicated by the fact that REBCO CCs are not a mature industrial product. Instead, CCs have defects and inconsistencies that can impact SCS distributions and coil survivability. Examples include fluctuations in $I_c(B,T,\theta)$ (and thus SCS magnitude) along and among tape lengths [4], edge degradation in the form of cracks (from mechanical slitting) or thermally-induced delamination (from laser slitting) that can reduce fatigue life [5], [6], [7], or geometric inhomogeneities which increase winding compressibility and exacerbate SCS [8], [9], [10].

		LBC1	LBC2	LBC3	LBC4	LBC6
Conductor	Specification	30 μm Hastelloy, 2 μm Ag, 5 μm Cu				
	Manufacturer	SuperPower				Shanghai
	REBCO Layer	GdBCO + BZO nanorods (MOCVD)				EuBCO + BaHfO3 nanoparticles (PLD)
	Edge slitting	Single- or double-slit mechanical			Single-slit mechanical	Double-slit laser
	Elastic modulus (E)	200 GPa (fully elastic); 160 GPa (Cu yielding)				165 GPa
	Yield stress (σ_y)	1000 MPa				815 MPa
	Irreversibility strain (ϵ_{irr})	0.45%				0.39%
	I_c range (4.2 K, 30 T, B//ab)	520 to 630 A				1200 to 1700 A
Coil	Conductor Orientation	Random			Low-SCS	Low-SCS
	Winding tension	<1 kgf				
	ID; OD [mm]	14; 34				14; 37
	Average # Turns	217	222	226	220	255
	Peak Field; Current	40.2 T; 163.4 A	42.5 T; 200.1 A	45.5 T; 245.5 A	44.0 T; 213.5 A	42.6 T; 170.0 A
	Operable after Quench	No	No	No	No	Yes

Fig. 1. *Left:* Basic parameters of LBC6 compared to LBC1—4. Conductor orientation can affect SCS via widthwise J_c gradients and *ab*-plane tilts, meaning that one winding orientation corresponds to lower SCS. *Right*: LBC6 before instrumentation.

"Dry-wound" test coils (without epoxy or solder consolidation) are important tools for investigating the impact of conductor properties on SCS and coil behavior. After a dry-wound coil is intentionally tested in a high-stress regime (typically SCS $>$ 800 MPa), it can be easily unwound to identify regions of plastic deformation ($\sigma > \sigma_y$, the yield stress) and I_c degradation ($\epsilon > \epsilon_{irr}$, the irreversibility strain). In combination with the coil test voltages, the observed damage patterns can be used to infer the experimental SCS distribution. Of particular interest are discrepancies between the experimental and calculated SCS, since this can indicate the presence of unappreciated CC property variations that modified SCS.

One type of dry-wound test coil used by our group for SCS experiments is the "Little Big Coil" (LBC). Each LBC follows a standardized design, comprising 12 dry wound no-insulation (NI) pancakes connected in series via low-resistance inner and outer joints, diagrammed schematically in Refs. [11] and [12]. To access a high-SCS regime, LBCs are ramped to quench at 4.2 K in the 31 T resistive background field at the National High Magnetic Field Laboratory (NHMFL).

The first four LBCs demonstrated a correlation in which pancakes wound from single-slit SuperPower AP conductor experienced no I_c degradation if the mechanically-slit edge was oriented towards the magnet midplane [11], [12], [13].

This work is supported by the U.S. Office of Fusion Energy Sciences Grant DE-SC0022011; by the U.S. Office of High Energy Physics Grant DE-SC0017657; and by the National High Magnetic Field Laboratory (NHMFL), which is supported by the National Science Foundation Cooperative Agreement No. DMR-2128556 and by the State of Florida. Author J. Lee was also supported by the Department of Defense (DoD) through the National Defense Science and Engineering Graduate (NDSEG) Fellowship Program.

At the time of this work, the authors were affiliated with the NHMFL and the FAMU-FSU College of Engineering, Tallahassee, FL 32310. Author G. Bradford is now affiliated with Advanced Conductor Technologies LLC, Boulder, CO 80301.

Manuscript received October 13, 2025; revised February 24, 2026.

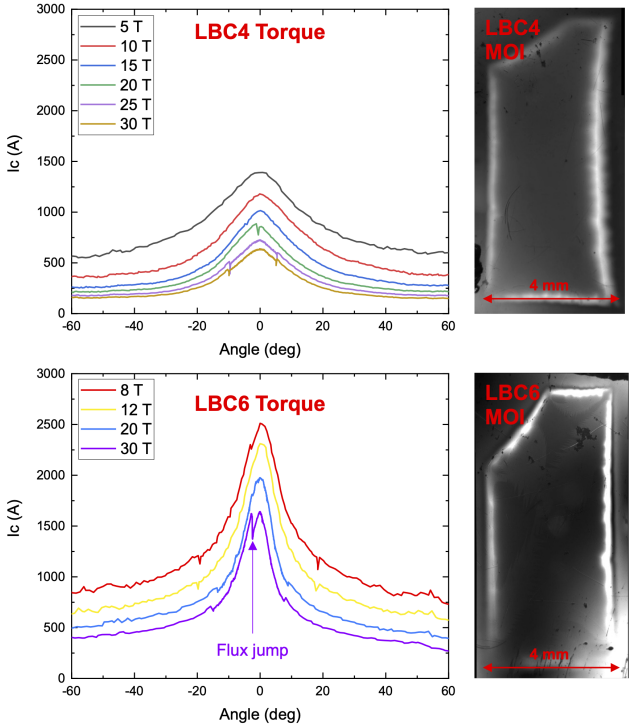

Fig. 2. Samples of conductor used in LBC1—4 vs. LBC6. *Left*: Torque magnetometry assessments of $I_c(B, \theta, 4.2\text{ K})$. Whereas $I_c(30\text{ T}, 4.2\text{ K}, B//ab) \sim 600$ A for the LBC1—4 conductor sample, it is more than 1500 A for this particular LBC6 conductor sample; this I_c was high enough to cause a flux jump during measurement. *Right:* Magneto-optical imaging (MOI) at 10 K, 50 mT. The LBC4 conductor shows deeper flux penetration into the right edge, indicating a widthwise J_c gradient. Meanwhile, the LBC6 conductor shows uniform penetration and no signs of a J_c gradient.

We originally hypothesized that damage was mitigated because this orientation placed mechanical slitting cracks on the compressive side of the SCS distribution, where they were unlikely to propagate. However, postmortem analysis indicated that the dominant variable was a widthwise J_c gradient in single-slit SuperPower AP tape, which narrowed the effective superconducting filament width. Relative to the J_c on the tape centerline, the J_c was 45% higher on the slit edge and fell to effectively zero on the non-slit edge, likely due to growth defects near the edge of the original 12 mm tape before slitting [14]. An important secondary variable was the small deviation (typically less than 5°) between the tape plane and the *ab*-plane of the REBCO layer; this is sometimes referred to as the "*ab*-plane offset." REBCO solenoids are often designed such that the field angle lies close to the tape plane, but since the *ab*-plane peak in $I_c(\theta)$ becomes narrow at high field, any unexpected deviation between the tape plane and the actual *ab*-plane peak can impact I_c and SCS [15], [16], [17]. The effect of both widthwise J_c variations and *ab*-plane offsets is that the SCS state can be modified by flipping the orientation with which a CC is wound into a coil [12], [18]. With the LBC1—4 conductor, orienting the slit edge towards the magnet midplane coincidentally accessed a low-SCS configuration. By accounting for these properties, we retroactively computed that the conductor would not have exceeded ϵ_{irr} under experimental conditions, as was observed.

Since the LBC1—4 tests, however, REBCO CCs have evolved. Driven by the requirements of the fusion industry, modern pinning landscapes eschew extended nanorods in favor of dense precipitate arrays, which are more amenable to mass production and which improve performance at low temperatures and high fields [19], [20], [21]. These developments are promising for the future of high-field magnets, but higher J_c permits larger screening currents, suggesting that these high-performance CCs might be more vulnerable to SCS damage than their predecessors. Furthermore, our group has internally observed that some recent CCs do not have widthwise J_c gradients, either due to fundamental differences in manufacturing technology (PLD vs. MOCVD) or improved process controls. This suggests that the orientation-based SCS mitigation technique in LBC1—4 might be less effective for contemporary CCs.

To begin exploring the relationship between conductor properties and SCS damage in these new CCs, we constructed LBC6* using conductor from Shanghai Superconductor Technologies (SST). Unlike LBC1—4, which were inoperable after quench, LBC6 remained electrically connected and was energized a total of 15 times in LHe, including 3 quenches from more than 42 T. Postmortem characterizations revealed that SCS damage was confined to one conductor edge. While the detailed analysis is not yet complete, we use this paper to present our preliminary findings and discuss a possible mechanism of self-limiting SCS damage that may have contributed to the coil's survivability.

II. Methods

A. Conductor Selection and Characterization

8 REBCO CCs from SST were procured according to specifications (laser-slit on both edges, 4 mm width, 30 µm Hastelloy substrate, and 5 µm Cu stabilizer). The tapes were scanned using YateStar, a reel-to-reel 77 K magnetization measurement system; the current configuration and limitations of YateStar are described in Ref. [18]. With the exception of occasional dropouts separated by several tens of meters, J_{cm}(77 K, self-field) varied by less than ±6% across the entire procurement. Short samples were measured using torque magnetometry [22] at variable fields (8–30 T) and temperatures (4.2–20 K) to assess $I_c(B, T, \theta)$. From these data, 2 tapes (labelled ST2210-137 and ST2210-129) were selected for coil construction. These tapes had similar $I_c(B, T, \theta)$ with a combined length (298 m) sufficient to wind the coil (260 m) with some spare length. Samples from the selected tapes were examined using magneto-optical imaging (MOI); no signs of widthwise I_c inhomogeneity were observed (see Fig. 2).

The selected tapes were divided into sections of 23 m, slightly more than the requisite length to wind each pancake. The *ab*-plane offsets of all sections were measured nondestructively using XRD. One section was additionally measured every 25 cm using our procedure from Ref. [18] to characterize fluctuations on a smaller length scale. The mean offsets of the two original tapes were slightly different ($\theta_{ab} = -1.6$°

*LBC5 was constructed using REBCO from Faraday Factory Japan (FFJ), but was destroyed by an accidental background magnet trip and did not produce meaningful results.

for ST2210-137 and $\theta_{ab} = +2.3$º for ST2210-129), but these offsets varied along each tape by less than ±0.15°.

One sample from each winding section was measured using torque magnetometry, thus producing $I_c(B, T, \theta)$ datasets corresponding to every 23 m along the original tapes. This afforded us a rough (non-statistical) parameterization of the homogeneity of $I_c(B, T, \theta)$ along the length. In the domain of interest around the *ab*-plane at 4.2 K, the torque magnetometry curves fell into an envelope with bounds parameterized by the modified Kim's fit [23], which takes account of Blatter's angular anisotropy factor [24]:

$$I_c(B, \theta) = I_{c0}\left(1 + \frac{\epsilon_\theta B}{B_0}\right)^{-\alpha} \quad (1)$$

$$\epsilon_\theta = \sqrt{k^2 \cos^2(\theta - \theta_{ab}) + \sin^2(\theta - \theta_{ab})} \quad (2)$$

Here $\theta = 0$º corresponds to B parallel to the tape plane. For the upper bound, $I_{c0} = 3500$ A, while for the lower bound, $I_{c0} = 2500$ A. The values $B_0 = 0.85$ T, $k = 0.05$, and $\alpha = 0.7$ were used for both bounds.

Attempts were made to corroborate the torque data with classic I-V transport measurements, but the transport samples burned after a single measurement due to a combination of high I_c, thin stabilizer, and mounting difficulties. For ST2210-139, the transport current at burnout (15 T, 4.2 K, 18°) was 613 A, while for ST2210-129 it was 619 A. These values were respectively 13.5% and 1.61% below the lower bound of the torque magnetometry envelope, likely due to sample heating from the current contacts preceding burnout.

The stress-strain constitutive relation of the conductor was measured via tensile test at 77 K, producing an elastic modulus of 165 GPa and a 0.2% yield stress of 815 MPa. We did not have the capabilities to perform tensile testing at the target coil operating temperature of 4.2 K, but based on literature results [25], [26], [27], we expected these values to increase by no more than ∼15% compared to 77 K. The strain irreversibility limit (ϵ_{irr}) was assessed using Walters spring measurements [28] at 77 K. After deconvolving bending and thermal strains, it was found that $\epsilon_{irr} = 0.39\%$.

B. Coil Construction

Each coil module comprised 2 pancake-wound tapes connected via an inner joint (an indium-soldered lap joint using 8 mm wide CC). Each module was wound onto the mandrel in the low-I_c configuration (*ab*-planes tilted away from the expected field direction) then compressed uniaxially at 800 kPa. Throughout construction, thin (0.127 mm) G10 spacers were added to prevent shorting between pancakes and the modules were tested at 77 K to ensure low resistances (less than 1 μΩ). Outer joints (also indium-soldered lap joints using 8 mm wide CC) were added between adjacent modules as well as to the top and bottom current leads, though the Module 1-to-2 and Module 4-to-5 outer joints had high resistances (31 μΩ and 25 μΩ at 77 K) and could not be repaired.

The coil was instrumented to track the voltages across each module and each outer joint. Cernox temperature sensors were installed at the top and bottom of the coil. A high-field calibrated Hall probe was installed in the coil center. Finally, the coil was affixed to a high-current probe and wrapped in Teflon tape, which decreased cooling efficiency but was necessary to protect the instrumentation leads during insertion into the cryostat and to avoid cryostat shorts. LBC6 and its design parameters are presented in Fig. 1.

C. Coil Test

LBC6 was installed in a LHe cryostat and centered in the field of the 31 T resistive outsert magnet. A dump resistor was installed between the current leads; however, given the 3 Ω resistance we expected that quenches would still be dominated by the coil's self-dissipating NI characteristics. The background field was increased to 31 T, after which the coil was energized incrementally at a ramp rate of 0.05 A/s. Quench occurred at 170 A (42.6 T center field). The data collected during this test are presented in Fig. 3. For comparison, the calculated coil I_c (lower bound parameters of Eq. 1) was 370 A, accounting for field angle but ignoring the effects of damage and heating. This means that the quench at 170 A occurred with a load line margin of 54%.

After the quench, LBC6 remained electrically connected and all modules retained low resistance. We decided to continue testing and the coil remained operational to the end of our allotted access to the 31 T background magnet. In total, LBC6 experienced 4 quenches, 2 accidental rapid discharges, and 9 cycles at variable ramp rates (0.05 A/s to 0.5 A/s). The voltage data from all ramps are not presented in this paper due to space limitations, but the basic parameters are summarized in Table I. In the table, "Quench" indicates that the ramp ended in quench, "Dump" indicates that we (accidentally) rapidly discharged the coil, and "Cycled" indicates that the coil was fully discharged without incident. Stationary resistance (150 A) refers to the resistance calculated from non-inductive voltages during a pause in the ramp at 150 A. The table does not include the 4 modules and 3 outer joints which showed negligible stationary resistance for the entirety of coil testing.

TABLE I
SUMMARY OF LBC6 COIL TESTS.

Ramp #	Background Field	Peak Current	Peak Field	Result	Stationary Resistance (μΩ) at 150 A					
					Mod 3	Mod 6	Term-Mod1 Outer Joint	Mod1-Mod2 Outer Joint	Mod5-Mod6 Outer Joint	Mod6-Term Outer Joint
1	31 T	170 A	42.6 T	Quench	0	0	1	41	20	1
2		120 A	39.0 T	Dump	*N/A (did not reach 150 A)*					
3		150 A	41.0 T	Dump	19	4	1	49	20	2
4			41.0 T	Cycled	19	4	1	47	19	2
5			41.0 T		19	4	1	48	19	3
6			41.0 T		19	4	1	48	19	3
Overnight warm-up to 200 K then cooldown to 4.2 K										
7	0 T	185 A	11.9 T	Quench	9	3	1	22	12	2
8		100 A	6.5 T	Cycled	*N/A (did not reach 150 A)*					
9	31 T	173 A	42.4 T	Quench	19	4	2	16	20	4
10		170 A	42.2 T	Quench	20	5	2	14	21	6
11		150 A	40.8 T	Cycled	19	5	2	15	21	6
12			40.8 T		19	5	2	17	21	6
13			40.7 T		19	5	2	18	20	6
14			40.9 T		20	5	2	19	21	7
15	0 T	150 A	9.7 T		9	3	1	25	13	5

= location of quench initiation

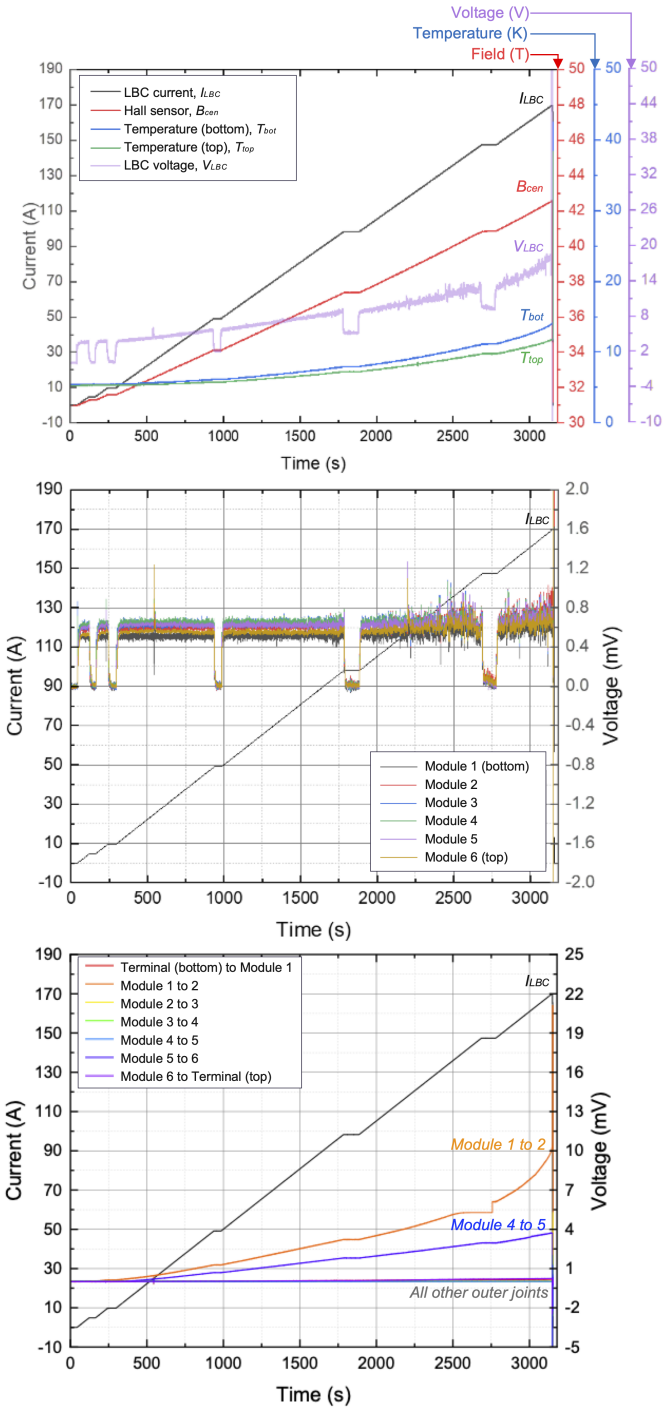

Fig. 3. Data from Ramp #1 of LBC6 in 31 T background. *Top:* Peak field, coil temperature, and total coil voltage (the sum across 6 modules and 7 outer joints). *Middle:* Individual voltages from the 6 modules. Each module voltage is the sum across 2 pancakes and 1 inner joint. *Bottom:* Individual voltages across the 7 outer joints. The flat voltage in the Module 1-2 outer joint between ∼2600s and ∼2750s was a data acquisition issue. Current is included on all graphs for reference.

D. Coil Postmortem

After high-field operation, the joints were removed and all pancakes unwound to allow visual observations of conductor deformation. The damaged conductor was scanned at 77 K using YateStar and samples were extracted from regions of interest. These samples were imaged magneto-optically (MOI) at 10 K, after which the overlayers were removed via brief exposures to aqueous solutions of $(NH_4)_2S_2O_8$ (Cu etchant) and $NH_4OH + H_2O_2$ (Ag etchant) so that the REBCO surface could be inspected using SEM.

E. Coil Simulation

SCS simulations of the coil used a COMSOL implementation of the model described in Refs. [12] and [29]. The model invokes the H-formulation with edge elements, domain homogenization, and an E-J power law with $n = 30$. For the simple initial treatment described in this paper, all modules used $J_c(B, \theta)$ corresponding to the upper bound parameters of Eq. 1. The measured elastic modulus at 77 K for the conductor was used to couple the electromagnetic treatment with a mechanical model. This version of the model does not account for heating or plastic deformation.

III. Results

Conductor damage was catalogued in all pancakes during unwinding, as presented in Fig. 4. In Pancakes 1—6 and 10—12, wavy plastic deformation was observed on the conductor edge facing away from the coil midplane. This damage became more pronounced towards the outer turns of the coil and resembled the SCS damage observed in LBC1—4. However, Pancakes 7—9 showed this waviness on the opposite edge. Since both edges of the conductor were laser-slit, this difference was unlikely to be related to edge defects; instead, it suggests a shift in magnet center and an inversion of SCS profile during quench. Furthermore, the damaged edge in the end pancakes (Pancakes 1 and 12) showed local buckling, extending up to 1 mm from the edge and occurring with a

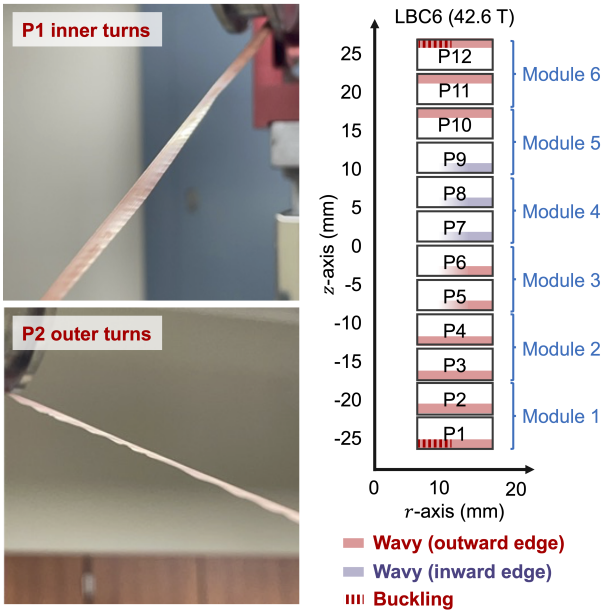

Fig. 4. Damage observed during LBC6 unwinding. *Top left:* Example of buckling from Pancake 1. This mode of damage became more severe towards the inner coil turns. *Bottom left:* Example of waviness from Pancake 2. This mode of damage became more severe towards the outer coil turns. *Right:* Diagram of types of damage observed in each pancake. Pancakes 7—9 showed waviness on the edge facing the coil midplane, suggesting an inversion of SCS during the experiment (likely during quench).

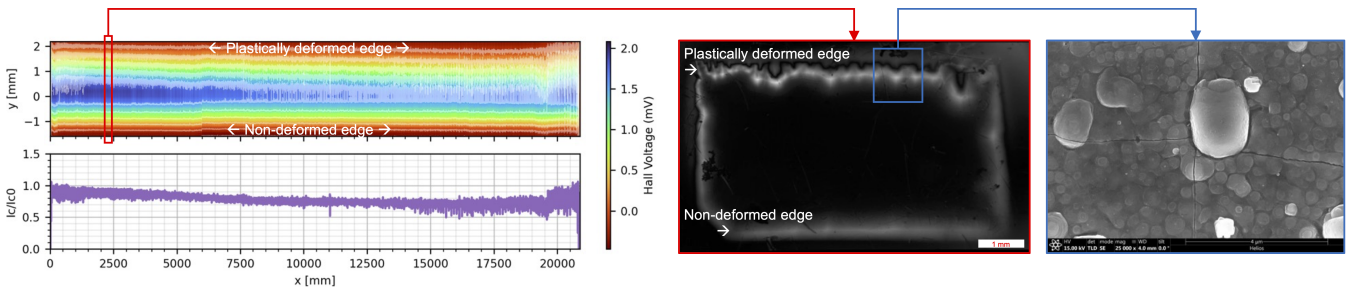

Fig. 5. Postmortem of damaged LBC6 conductor. *Left:* YateStar magnetization map and reconstructed I_c of Pancake 1, normalized to the I_c of the original conductor before high-field operation. On the magnetization map, the smooth gradient on the bottom edge indicates no damage, while the interrupted gradient on the top edge indicates damage. *Middle:* MOI image of a sample corresponding to the boxed region of the YateStar scan. Flux salients extend ∼1 mm into the damaged edge of the sample. *Right:* SEM image taken from the boxed region of the MOI sample after etching Cu and Ag overlayers. The region is cracked but no signs of delamination are observed. All pancakes show similar features to Pancake 1, i.e., degradation and cracking confined to a single edge of the conductor.

period of a few mm, which became more prominent towards the inner windings.

YateStar scans of the damaged conductor correlated the plastic deformation with local damage to the superconducting layer. However, this damage was always confined to one edge; the non-deformed edge showed no interruption in superconductivity. MOI examination of short samples corroborated these features at 10 K: throughout all short samples examined, the plastically deformed edge showed salients of flux penetration up to 1 mm into the tape, indicating localized damage to the superconducting layer. Meanwhile, the non-deformed edge showed no sign of damage.

SEM inspection revealed that the damage detected by YateStar and MOI corresponded to cracks in the REBCO layer. These cracks generally followed a grid-like pattern and often bisected particulates in the REBCO layer without interruption. Other than the cracks, the REBCO surface morphology in the damaged regions resembled that of the undamaged edge and of other etched SST samples. This suggested that no material was lost during etching and that, even when fractured, the oxide layers in this CC did not readily delaminate.

YateStar, MOI, and SEM results from Pancake 1 are presented in Fig. 5. Similar features were observed across all 12 pancakes during the postmortem.

IV. Discussion

A. Expectation of SCS Damage in LBC6

Based on the measured conductor properties, we expected LBC6 to experience I_c degradation during energization. Compared to the LBC1—4 conductor, the LBC6 conductor had 3x larger I_c and no widthwise gradients in I_c that might be leveraged for SCS mitigation (see Fig. 2). Furthermore, comparing the 77 K mechanical properties, the LBC1—4 and LBC6 conductors had a similar elastic modulus but different irreversibility strains (0.45% vs. 0.39%) and 0.2% offset yield stresses (1000 MPa vs. 815 MPa). The combination of larger SCS and lower mechanical limits suggested that LBC6 would encounter its ϵ_{irr} at lower operating currents than LBC1—4. Simulations indicated that degradation would begin around an operating current of 30 A, though in practice it was difficult to identify the onset of damage within the coil test voltages.

B. Dissipation and Degradation During Quench and Cycling

The data collected during the first ramp of LBC6 are shown in Fig. 3. The data show simultaneous voltage spikes across all modules that become more frequent at high currents and fields. Similar features were observed during all ramps in 31 T background field. These events indicate current redistribution, but it is unclear if the cause was flux jumps, abrupt conductor motion, conductor damage, or a combination thereof.

At the onset of the first quench, the total coil voltage was 18 mV, but the module voltages were all approximately 0.7 mV and inductive in nature. The rest of the coil voltage was the result of dissipation in the Module 1-to-2 outer joint (10 mV) and the Module 4-to-5 outer joint (4 mV), which were the joints that showed higher resistances than other coil components after construction. The quench appears to have initiated in the Module 1-to-2 outer joint, as evidenced by the super-linear increase in its voltage above 150 A. This joint also caused the second quench (Ramp #7).

LBC6 remained electrically connected throughout testing, but the voltage data suggested degradation with repeated operation. The stationary resistances in the top- and bottom-most outer joints started below 1 μΩ, but they rose to 2 μΩ and 7 μΩ by the final high-field ramp, suggesting that our simple outer joint design is vulnerable to fatigue in the high-SCS regions of the coil. Furthermore, Modules 3 and 6 were damaged by the initial quench and subsequently showed resistances of 19 μΩ and 4 μΩ, respectively. The damage in Module 3 appears to have initiated the third and fourth quenches (Ramps #9 and #10). Interestingly, despite the different initiation sites, all quenches occurred at similar currents, which may be related to fundamental cooling limitations of the coil geometry.

While there exist multiple examples of high-field REBCO solenoids surviving quench and cycling from above 30 T without degradation [30], [31], LBC6 is to our knowledge the first example of a REBCO test coil that endured repeated quenches from $B > 40$ T. On one hand this is unsurprising due to the coil's small size and low stored energy. However, such a result is a departure from LBC1—4, all of which were rendered inoperable upon quench from above 40 T. Some of the difference can be explained in terms of accrued experience in coil fabrication, but conductor properties may have also played a role via a self-arresting SCS mechanism, discussed in the next subsection.

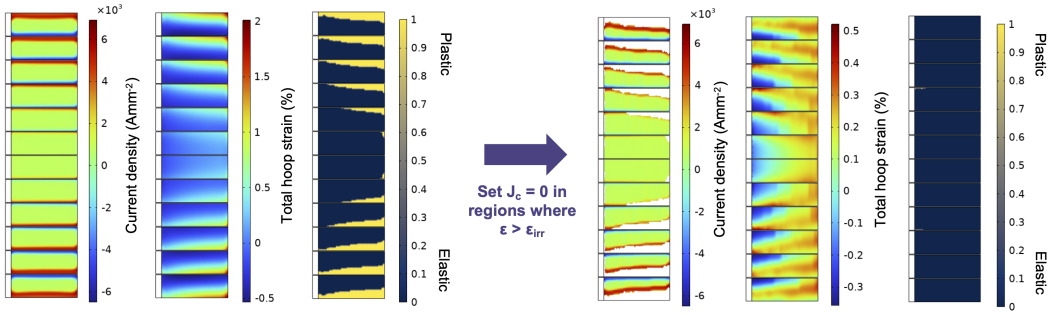

Fig. 6. Simulation study of self-arresting SCS damage in LBC6. Left: Simulation of LBC6 energized to its peak current of 170 A (31 T background). The regions of the winding pack that exceed $\epsilon_{irr} = 0.39\%$, and thus experience I_c degradation, are marked in yellow. Right: After setting $J_c = 0$ in the regions that exceeded ϵ_{irr}, the simulated LBC6 was again energized to 170 A (31 T background). No additional regions were found to exceed ϵ_{irr}.

C. A Possible Mechanism of Self-Arresting SCS Damage

Given that LBC6 was energized 15 times in LHe, it was not possible to directly correlate the observed conductor damage to any specific event in the test campaign. However, based on our understanding of SCS in REBCO magnets, we reasoned that SCS would be highest with undamaged conductor and thus that damage would be most likely to occur during the first coil energization and quench (as evidenced by the increased resistances in Modules 3 and 6 after the first quench). We therefore considered how the coil could continue operating for 14 additional energizations despite conductor damage.

Since the postmortem revealed that I_c degradation was confined to one conductor edge, we propose that in the LBC6 test, SCS damage was self-arresting. During the initial ramp-up of the undamaged coil, high SCS caused one conductor edge to exceed its irreversible strain limit (0.39%). The REBCO layer on that edge cracked and was no longer able to locally carry current. In turn, this damage narrowed the current-carrying width and decreased SCS until an equilibrium state was established. This type of localized damage has been considered as a possible means of SCS mitigation in the NHMFL 32 T project [32], but to our knowledge has not yet been addressed directly in literature. LBC6 may represent an example of this self-arresting mechanism.

As a simple numerical examination of the proposed mechanism, we simulated two LBC6 energizations, the results of which are presented in Fig. 6. First, we simulated the energization of the undamaged coil, which caused one edge of the *in silico* conductor to exceed the 0.39% irreversible strain limit due to SCS. We then set $J_c = 0$ A/mm^2 in these regions, corresponding to cracks in the REBCO, and simulated a second energization to the same operating current. No further regions of the *in silico* conductor exceeded 0.39% strain. In other words, SCS destroyed one conductor edge during the initial ramp, such that in subsequent ramps, SCS was reduced and no further damage could occur. Because the original conductor had a high I_c margin, enough I_c was retained for the coil to reach the same operating current in both simulations.

These numerical results are an oversimplification given that conductor damage, strain hardening, and SCS redistribution would occur simultaneously during coil energization. Another oversimplification is our use of a uniaxial value of ϵ_{irr}, since the real stress state in LBC is triaxial. Furthermore, it is not clear how the first quench (with its associated overcurrents) contributed to the conductor damage or if other properties of SST CCs helped arrest SCS damage. We are upgrading our numerical treatment and conductor characterization capabilities to explore these questions.

We note a similarity between the damaged LBC6 conductor and the undamaged LBC1—4 conductor. In both cases, the effective current-carrying width is narrower than the tape width. Our simulations in Fig. 6 and Ref. [12] indicate that this feature mitigates SCS damage; our test data and postmortem characterizations are consistent with these calculations. Both results suggest that to optimize CCs for operation in ultra-high-field environments, it may be beneficial to intentionally introduce a J_c gradient and/or reduce the width of the REBCO layer relative to the tape width so as to mitigate SCS. This might be accomplished during deposition by, e.g., masking the substrate or introducing widthwise temperature gradients. Alternatively, magnet designers might intentionally damage one conductor edge before coil winding. Finally, the feature may be introduced *in situ* by allowing SCS to drive one conductor edge over ϵ_{irr} during the first energization and quench, as appears to have occurred in LBC6.

V. Conclusion

In this paper, we presented initial test and postmortem results of LBC6, a dry-wound REBCO test coil that reached 42.6 T in a 31 T background field. I_c degradation due to screening current stresses (SCS) was predicted and observed, but the coil repeatedly operated and quenched from more than 42 T despite the presence of this damage. Postmortem characterization indicated that I_c degradation was confined to one conductor edge. We propose that this coil demonstrated a self-arresting SCS mechanism wherein the SCS damage incurred during the first energization narrowed the superconducting filament width, thereby reducing SCS and preventing damage during subsequent energizations. Such behavior suggests that a REBCO CC optimized for high-field magnets might intentionally incorporate this design feature to mitigate SCS.

Acknowledgments

We thank Dr. D. Abraimov, Dr. A. Ingrole, E. Marks, and J. Kvitkovic for measurement assistance; as well Dr. T. Mato, Dr. S. Noguchi, and Dr. S. Hahn for helpful discussions.

REFERENCES

[1] Z. Jiang, D. Jiang, X. Wu, W. Chen, and G. Kuang, "Numerical Research of Potential Methods to Reduce Screening-Current-Induced Stress for No-Insulation REBCO Coils," en, *IEEE Transactions on Applied Superconductivity*, vol. 32, no. 5, pp. 1–14, Aug. 2022, ISSN: 1051-8223, 1558-2515, 2378-7074. DOI: 10.1109/TASC.2022.3171260.

[2] Y. Suetomi et al., "Screening Current Induced Stress/Strain Analysis of High Field REBCO Coils With Co-Winding or Over-Banding Reinforcement," *IEEE Transactions on Applied Superconductivity*, vol. 34, no. 5, pp. 1–6, Aug. 2024, ISSN: 1558-2515. DOI: 10.1109/TASC.2023.3342762.

[3] R. Slade, R. Bateman, G. Brittles, M. Bristow, J. Van Nugteren, and B. Van Nugteren, *HTS Magnet Ramping to Reduce Screening Currents*, Jan. 2025.

[4] X. Hu et al., "An Experimental and Analytical Study of Periodic and Aperiodic Fluctuations in the Critical Current of Long Coated Conductors," en, *IEEE Transactions on Applied Superconductivity*, vol. 27, no. 4, pp. 1–5, Jun. 2017, ISSN: 1051-8223, 1558-2515. DOI: 10.1109/TASC.2016.2637330.

[5] C. Guo et al., "Enhancement of electro-mechanical behaviors in RE–Ba–Cu–O composite superconducting tapes with laser slit edges," en, *Superconductor Science and Technology*, vol. 35, no. 11, p. 115 009, Nov. 2022, ISSN: 0953-2048, 1361-6668. DOI: 10.1088/1361-6668/ac96d5.

[6] G. Bradford, J. Jaroszynski, G. Murphy, A. Polyanskii, J. Lee, and D. C. Larbalestier, "Property Variations in Modern REBCO Coated Conductors from Multiple Manufacturers," en, *IOP Conference Series: Materials Science and Engineering*, vol. 1302, no. 1, p. 012 011, May 2024, Publisher: IOP Publishing, ISSN: 1757-899X. DOI: 10.1088/1757-899X/1302/1/012011.

[7] G. Vernassa, *Performance limitations of UHF REBCO solenoids*, CERN, Meyrin, Switzerland, Nov. 2025.

[8] J. Park et al., "Numerical Study on Effect of Boundary Conditions and Winding Compressibility on Screening Current Induced Stress," *IEEE Transactions on Applied Superconductivity*, vol. 35, no. 5, pp. 1–5, Aug. 2025, ISSN: 1558-2515. DOI: 10.1109/TASC.2025.3538680.

[9] S. R. Griffin et al., "Measured and Simulated Strain in the Large Scale Coil With Considering Winding Compressibility," *IEEE Transactions on Applied Superconductivity*, vol. 36, no. 3, pp. 1–5, May 2026, ISSN: 1558-2515. DOI: 10.1109/TASC.2025.3630115.

[10] Y. Suetomi et al., "Screening Current-Induced Stress and Strain Analysis Considering a Non-uniform Thickness Profile of REBCO Tapes," *IEEE Transactions on Applied Superconductivity*, vol. 36, no. 3, pp. 1–6, May 2026, ISSN: 1558-2515. DOI: 10.1109/TASC.2025.3637739.

[11] S. Hahn et al., "45.5-tesla direct-current magnetic field generated with a high-temperature superconducting magnet," en, *Nature*, vol. 570, no. 7762, pp. 496–499, Jun. 2019, ISSN: 0028-0836, 1476-4687. DOI: 10.1038/s41586-019-1293-1.

[12] J. Bang et al., "Evidence that transverse variability of critical current density can greatly mitigate screening current stress in high field REBCO magnets," en, *Scientific Reports*, vol. 14, no. 1, p. 31 703, Dec. 2024, Publisher: Nature Publishing Group, ISSN: 2045-2322. DOI: 10.1038/s41598-024-81902-0.

[13] X. Hu et al., "Analyses of the plastic deformation of coated conductors deconstructed from ultra-high field test coils," en, *Superconductor Science and Technology*, vol. 33, no. 9, p. 095 012, Sep. 2020, ISSN: 0953-2048, 1361-6668. DOI: 10.1088/1361-6668/aba79d.

[14] M. Solovyov et al., "Non-uniformity of coated conductor tapes," en, *Superconductor Science and Technology*, vol. 26, no. 11, p. 115 013, Oct. 2013, ISSN: 0953-2048. DOI: 10.1088/0953-2048/26/11/115013.

[15] J. Lu, Y. Xin, Y. Zhang, and H. Bai, "Ab-Plane Tilt Angles in REBCO Conductors," *IEEE Transactions on Applied Superconductivity*, vol. 33, no. 5, pp. 1–4, Aug. 2023, Conference Name: IEEE Transactions on Applied Superconductivity, ISSN: 1558-2515. DOI: 10.1109/TASC.2023.3236258.

[16] D Kolb-Bond et al., "Screening current rotation effects: SCIF and strain in REBCO magnets," en, *Superconductor Science and Technology*, vol. 34, no. 9, p. 095 004, Sep. 2021, ISSN: 0953-2048, 1361-6668. DOI: 10.1088/1361-6668/ac1525.

[17] J. L. Cheng et al., "Statistics on *ab*-Plane Offsets in REBCO Coated Conductors and Implications for Non-Twisted Magnets," en, *IEEE Transactions on Applied Superconductivity*, vol. 35, no. 5, pp. 1–6, Aug. 2025, ISSN: 1051-8223, 1558-2515, 2378-7074. DOI: 10.1109/TASC.2025.3545023.

[18] J. Lee, J. Bang, G. Bradford, D. Abraimov, E. Bosque, and D. Larbalestier, "Lengthwise Characterizations of Crystallographic Tilt in Contemporary REBCO Coated Conductors," *IEEE Transactions on Applied Superconductivity*, vol. 35, no. 5, pp. 1–5, Aug. 2025, ISSN: 1558-2515. DOI: 10.1109/TASC.2024.3505115.

[19] A. Molodyk et al., "Development and large volume production of extremely high current density $YBa_2Cu_3O_7$ superconducting wires for fusion," en, *Scientific Reports*, vol. 11, no. 1, p. 2084, Dec. 2021, ISSN: 2045-2322. DOI: 10.1038/s41598-021-81559-z.

[20] D. Abraimov et al., "Optimization of Transport Critical Currents at 4.2 K – 20 K at Magnetic Fields Up to 31 T for MOCVD REBCO Conductors With Variable Zr and Growth Conditions," *IEEE Transactions on Applied Superconductivity*, vol. 35, no. 5, pp. 1–7, Aug. 2025, ISSN: 1558-2515. DOI: 10.1109/TASC.2025.3549409.

[21] A. Xu et al., "A Comprehensive Characterization of Commercial Pulsed Laser Deposited Coated Conductors," *IEEE Transactions on Applied Superconductivity*, vol. 35, no. 5, pp. 1–6, Aug. 2025, ISSN: 1558-2515. DOI: 10.1109/TASC.2025.3538638.

[22] J Jaroszynski et al., "Rapid assessment of REBCO CC angular critical current density J_c (B, T = 4.2 K, θ) using torque magnetometry up to at least 30 tesla," en, *Superconductor Science and Technology*, vol. 35, no. 9, p. 095 009, Sep. 2022, ISSN: 0953-2048, 1361-6668. DOI: 10.1088/1361-6668/ac8318.

[23] X Zhang, Z Zhong, H. S. Ruiz, J Geng, and T. A. Coombs, "General approach for the determination of the magneto-angular dependence of the critical current of YBCO coated conductors," en, *Superconductor Science and Technology*, vol. 30, no. 2, p. 025 010, Feb. 2017, ISSN: 0953-2048, 1361-6668. DOI: 10.1088/1361-6668/30/2/025010.

[24] G. Blatter, M. V. Feigel'man, V. B. Geshkenbein, A. I. Larkin, and V. M. Vinokur, "Vortices in high-temperature superconductors," en, *Reviews of Modern Physics*, vol. 66, no. 4, pp. 1125–1388, Oct. 1994, ISSN: 0034-6861, 1539-0756. DOI: 10.1103/RevModPhys.66.1125.

[25] C Barth, G Mondonico, and C Senatore, "Electro-mechanical properties of REBCO coated conductors from various industrial manufacturers at 77 K, self-field and 4.2 K, 19 T," en, *Superconductor Science and Technology*, vol. 28, no. 4, p. 045 011, Apr. 2015, ISSN: 0953-2048, 1361-6668. DOI: 10.1088/0953-2048/28/4/045011.

[26] K. Osamura, S. Machiya, Y. Tsuchiya, and H. Suzuki, "Internal Strain and Mechanical Properties at Low Temperatures of Surround Cu Stabilized YBCO Coated Conductor," en, *IEEE Transactions on Applied Superconductivity*, vol. 20, no. 3, pp. 1532–1536, Jun. 2010, ISSN: 1051-8223, 1558-2515. DOI: 10.1109/TASC.2010.2042437.

[27] S. Awaji et al., "Robust REBCO Insert Coil for Upgrade of 25 T Cryogen-Free Superconducting Magnet," *IEEE Transactions on Applied Superconductivity*, vol. 31, no. 5, pp. 1–5, Aug. 2021, ISSN: 1558-2515. DOI: 10.1109/TASC.2021.3061896.

[28] N. Cheggour and D. P. Hampshire, "A probe for investigating the effects of temperature, strain, and magnetic field on transport critical currents in superconducting wires and tapes," en, *Review of Scientific Instruments*, vol. 71, no. 12, pp. 4521–4530, Dec. 2000, ISSN: 0034-6748, 1089-7623. DOI: 10.1063/1.1324734.

[29] J. Bang, G. Bradford, K. Kim, J. Lee, A. Polyanskii, and D. Larbalestier, "Elastic-plastic conductor damage evaluation at over 0.4% strain using a high-stress REBCO coil," en, *Superconductor Science and Technology*, vol. 37, no. 9, p. 095 011, Sep. 2024, ISSN: 0953-2048, 1361-6668. DOI: 10.1088/1361-6668/ad6a9d.

[30] H. W. Weijers, "Magnet technology in the NHMFL 32 T HTS-LTS solenoid," en, 2014.

[31] Y Suetomi et al., "Quench and self-protecting behaviour of an intra-layer no-insulation (LNI) REBCO coil at 31.4 T," en, *Superconductor Science and Technology*, vol. 34, no. 6, p. 064 003, Jun. 2021, ISSN: 0953-2048, 1361-6668. DOI: 10.1088/1361-6668/abf54e.

[32] M. Bird, personal communication, Dec. 4, 2025.